

# Energy Flux due to Electromagnetic Fluctuations during Guide Field Magnetic Reconnection<sup>\*)</sup>

Akihiro KUWAHATA, Michiaki INOMOTO, Ryoma YANAI<sup>1)</sup> and Yasushi ONO

*The University of Tokyo, Kashiwa 277-8561, Japan*

<sup>1)</sup>*The University of Tokyo, Tokyo 113-0032, Japan*

(Received 11 January 2016 / Accepted 19 March 2016)

Large electromagnetic fluctuations inside the current sheet and large reconnection electric fields are observed during fast magnetic reconnection in the presence of a guide field. The fluctuations transport 2.5% of the dissipated magnetic energy from the reconnection region. Although the energy gains of the ions and electrons are approximately 60% and 12%, respectively, of the dissipated magnetic energy after the fast reconnection, the energy of fluctuations is not comparable to their energy gains. The fluctuations do not directly contribute to the energy conversion but might cause the fast reconnection leading to the rapid release of magnetic energy.

© 2016 The Japan Society of Plasma Science and Nuclear Fusion Research

Keywords: electromagnetic fluctuation, guide field magnetic reconnection, fast reconnection, energy conversion, ion heating and acceleration

DOI: 10.1585/pfr.11.1301087

Magnetic reconnection is a fundamental phenomenon that occurs in all magnetized plasmas: solar flare, magnetosphere, and laboratory plasmas [1, 2]. The energy release rate, for example, in solar flares, is much higher than that estimated by the Sweet-Parker model [3, 4] with the Spitzer resistivity [5, 6]. Fast reconnection involves the release of a huge amount of magnetic energy leading to particle acceleration and heating.

Various electromagnetic fluctuations, such as waves and instabilities, have been considered to play a key role in the rapid energy release processes [7–9]. In the magnetosphere and solar plasmas, the electromagnetic and electrostatic fluctuations, which are Alfvénic waves at small scales, are often observed during magnetic reconnection [9]. These waves may be important in coronal heating and the acceleration of solar wind [10]. In this paper, we report the experimental study of the energy conversion including electromagnetic fluctuations during guide field magnetic reconnection.

The magnetic reconnection experiment was conducted on the TS-3 plasma merging device at the University of Tokyo [11–14]. The vacuum vessel is cylindrical and its inner radius is 375 mm. The axial length of the vacuum chamber is approximately 1.0 m. Figure 1 shows a poloidal cross-section of TS-3. The EF coils are used to control the radial location of the current sheet and to confine plasma away from the inside walls by balancing the radial hoop force. The PF coils inside the TS-3 are wound toroidally to generate the two spherical tori by the swing of PF coil currents. The two torus plasmas come close to each other and

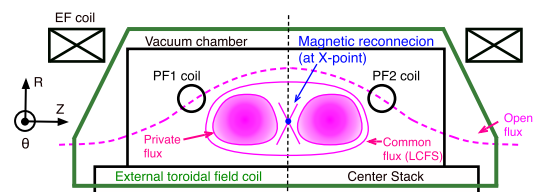


Fig. 1 Schematics of the TS-3 plasma merging device. Reconnection inflow and outflow are in the  $R$  and  $Z$  directions, respectively. Two torus plasmas collide and merge through magnetic reconnection at the center of the vacuum vessel ( $Z = 0$  mm: mid-plane).

collide, and then magnetic reconnection occurs at the mid-plane (center of the TS-3 on the axial direction:  $Z = 0$  mm). During magnetic reconnection, the external toroidal field ( $B_\theta$ ) generated by the axial current ( $I_Z$ ) acts a guide field  $B_{\text{guide}}$ . Hydrogen plasmas were employed in this experiment.

Typical plasma parameters during plasma merging via magnetic reconnection with guide fields in TS-3 are as follows: major radius is  $R_0 \sim 190$  mm, minor radius is  $a \sim 150$  mm, the strength of the reconnection magnetic field  $B_{\text{rec}}$  is 25 mT and the applied guide field  $B_{\text{guide}}$  is 60 mT, resulting in the guide field ratio of  $B_{\text{guide}}/B_{\text{rec}} \sim 2.5$ . The typical electron temperature  $T_e$  and density  $n_e$  measured by a Langmuir probe are 3–10 eV and  $0.2\text{--}2 \times 10^{20} \text{m}^{-3}$ , respectively. The ion temperature  $T_i$  deduced from a neutral line ( $H_\beta$ : 486.135 nm) spectrum measured using the IDSP (ion dynamics spectroscopy probe [15]) is 3–35 eV. Note that this emission line is reasonable for the ion Doppler spectroscopy in this experiment because the collision time

author's e-mail: kuwahata@bee.t.u-tokyo.ac.jp

<sup>\*)</sup> This article is based on the invited talk at the 32nd JSPF Annual Meeting (2015, Nagoya).

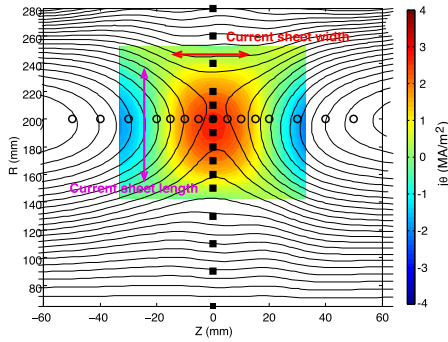


Fig. 2 Magnetic flux  $\Psi$  contour (solid lines) and out-of-plane current density  $j_\theta$  (color coded) during magnetic reconnection with guide field ratio  $B_{\text{guide}}/B_{\text{rec}} \sim 2.5$ , where the poloidal magnetic flux  $\Psi$  is given by  $\Psi = \int_{R_0}^R 2\pi R' B_Z dR'$  and the current density is given by  $j_\theta = (\partial B_R/\partial Z - \partial B_Z/\partial R)/\mu_0$ . The markers indicate the location of high-frequency pickup coils to measure the fluctuation of the reconnecting magnetic field  $B_R$  (open circles) and the reconnected magnetic field  $B_Z$  (solid squares).

between  $H^+$  and  $H$  is much shorter than the reconnection time scale [16]. The ion flow velocity measured by a Mach probe is  $-30$ - $40$  km/s. The current sheet width ( $\delta \sim 20$ - $40$  mm) and length ( $L \sim 60$ - $80$  mm) are larger than the ion gyroradius ( $\rho_i \sim 5$ - $10$  mm), electron gyroradius ( $\rho_e < 1$  mm), and electron skin depth ( $d_e < 1$  mm), and are comparable to the ion skin depth ( $d_i \sim 20$ - $40$  mm).

Figure 2 shows the poloidal flux  $\Psi$  and the current density  $j_\theta$  measured by a 2-D magnetic probe array [11,12] during guide field magnetic reconnection. Inflow comes from the left and right sides of the reconnection region, and outflow ejects to the top and bottom of the region. Two linear arrays of high-frequency pickup coils are used to measure the electromagnetic fluctuations as shown in Fig. 2. The effective frequency response is up to 20 MHz. An axial probe array (open circles) can obtain the magnetic fluctuation in the reconnecting component with spacings of 5-10 mm, and a radial probe array (solid squares) can measure the fluctuation in the reconnected component with spacings of 10-20 mm.

Figure 3 shows the time traces of the fluctuation raw signals  $\delta B_Z$  measured at 16 radial locations during magnetic reconnection with the guide fields. Electromagnetic fluctuations are observed inside the diffusion region and propagate to the downstream region ( $R \sim 150$  and  $230$  mm) from the vicinity of the X-point ( $R \sim 190$  mm) at  $t \sim 193$ - $194$   $\mu\text{s}$ . Our previous study [13] reports that the fluctuations have the feature of kinetic Alfvén wave (KAW): the peak frequency is  $1.5$ - $2$  MHz  $\sim 1.5 - 2f_{ci}$ , where  $f_{ci}$  is the local ion cyclotron frequency at the X-point, the parallel ( $\theta$ -direction) and perpendicular ( $R$ -direction) phase velocities are approximately  $92 \pm 5$  and  $50 \pm 10$  km/s, respectively. In this paper, we will focus on the role of fluctuations as the energy carrier from the reconnection region to

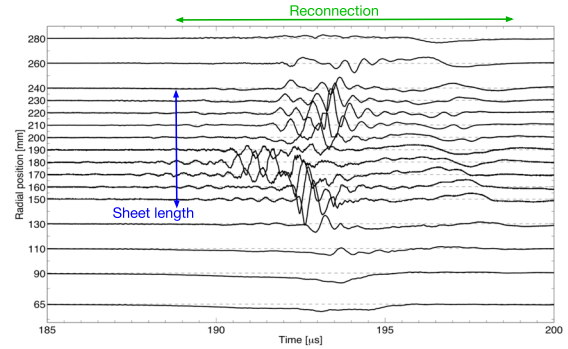


Fig. 3 Typical electromagnetic fluctuations  $\delta B_Z$  during magnetic reconnection with guide field  $B_{\text{guide}}/B_{\text{rec}} \sim 2.5$ . Signals are measured at 16 radial locations of the mid-plane. Large fluctuations are observed inside the current sheet at  $t \sim 192$ - $194$   $\mu\text{s}$ .

the downstream region.

It is commonly known that magnetic energy is converted to the kinetic/thermal energy through magnetic reconnection [17, 18]. To interpret the energy conversion processes during magnetic reconnection, incoming/outgoing energy flux into/from the reconnection region during reconnection are evaluated quantitatively.

Figure 4 shows the time evolution of the reconnection electric field  $E_\theta$  at the X-point and the Poynting flux into/out-of the reconnection region, where  $E_\theta = -1/(2\pi R)d\Psi/dt$ . The driven magnetic reconnection occurs in 185-198  $\mu\text{s}$ . The electric field increases up to 1000 V/m at  $t \sim 193$ - $194$   $\mu\text{s}$ , i.e., fast reconnection occurs. During this period, large electromagnetic fluctuations are generated inside the current sheet and propagate to the downstream region [see Fig. 3]. The incoming Poynting flux is approximately  $4 \times 10^7$  [W/m<sup>2</sup>] during this phase. The increment of outgoing flux is, however, not significant. We define this fast reconnection phase ( $t = 193$ - $194$   $\mu\text{s}$ ) as “phase 1” to focus on the energy of electromagnetic fluctuations. In addition, the occurrence of fast reconnection and the generation of large fluctuations clearly occur simultaneously as shown in Figs. 3 and 4, indicating that the fluctuations might cause the fast reconnection as previously reported [13]. “Phase 2” ( $t = 196$ - $197$   $\mu\text{s}$ ) is the latter phase of reconnection and is a relatively steady phase. The reconnection electric field ( $\sim 500$  V/m) and incoming Poynting flux ( $\sim 2 \times 10^7$  [W/m<sup>2</sup>]) are almost constant. No significant fluctuations are observed in phase 2 as shown in Fig. 3. In this phase, we focus on the ion’s energy gain because the highest ion temperatures are measured [see Fig. 5]. Because the durations when the fluctuations generate are 1-2  $\mu\text{s}$  as shown in Fig. 3, the time averaged period of 1  $\mu\text{s}$  for their phases is proper to estimate the energy focused on the fluctuations.

Figure 5 shows the radial profiles on the mid-plane ( $Z = 0$  mm) in the direction of the reconnection outflow of the

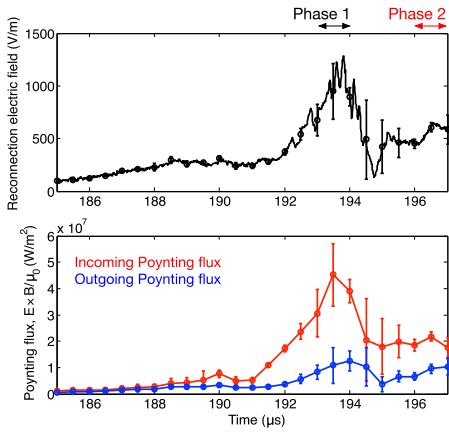


Fig. 4 Time evolution of (top) the reconnection electric field  $E_\theta$  at the X-point and (bottom) Poynting fluxes  $\mathbf{P} = \mathbf{E} \times \mathbf{B}/\mu_0$  through the reconnection region. Red and blue lines indicate the incoming and outgoing fluxes, respectively. To investigate the energy flow process, the reconnection duration is divided into two phases: phase 1 ( $t = 193 - 194 \mu\text{s}$ ) and phase 2 ( $t = 196 - 197 \mu\text{s}$ ). The errors are from the variation of several discharges.

ion temperature  $T_i$ , ion flow velocity  $V_i$ , electron temperature  $T_e$ , and electron density  $n_e$  measured in phase 1 ( $t = 193 - 194 \mu\text{s}$ ) and phase 2 ( $t = 196 - 197 \mu\text{s}$ ) of magnetic reconnection. Ion temperatures  $T_i$  are measured at  $R = 70 - 280 \text{ mm}$  (radial scan with a spacing of  $30 \text{ mm}$  conducted on shot by shot) by using the IDSP as shown in Fig. 5 (a). Ion heating occurs at the downstream region ( $R \sim 160$  and  $220 \text{ mm}$ ) in phase 2. The ion temperature at the inboard and outboard side increases to approximately  $20 \text{ eV}$  and  $10 \text{ eV}$ , respectively, from  $3 - 4 \text{ eV}$ . The ion flow velocity is measured using a Mach probe. A Mach probe can measure the ion Mach number  $M_i$ , and the ion flow velocity can be calculated by the equation  $V_i = M_i C_s$ , where  $C_s$  is the ion sound velocity. During magnetic reconnection, as shown in Fig. 5 (b), ions are radially accelerated up to  $30 - 40 \text{ km/s}$  around the downstream region  $R \sim 160$  and  $250 \text{ mm}$  in phase 2. The outflow velocity is comparable to the  $30\% - 40\%$  of the Alfvén velocity. Figures 5 (c) and (d) show the radial profiles of the electron temperature and the electron density, respectively. Unlike the ion temperature, no clear sign of electron heating is observed in this experiment. Regarding the electron density in phase 2, however, a significant increase caused by the outflow plasmas is observed in the downstream region.

To investigate the energy flow process, the following equations are used to evaluate the inflow/outflow energy fluxes to/from the reconnection region based on the electric field  $\mathbf{E}$ , magnetic field  $\mathbf{B}$ , and flow velocity  $\mathbf{V}$ :

$$\mathbf{P}_{\text{mag}} = E_\theta \mathbf{B}_R / \mu_0 \text{ (in) or } E_\theta \mathbf{B}_Z / \mu_0 \text{ (out)}, \quad (1)$$

$$\mathbf{K} = \frac{1}{2} m n V^2 \mathbf{V}, \quad (2)$$

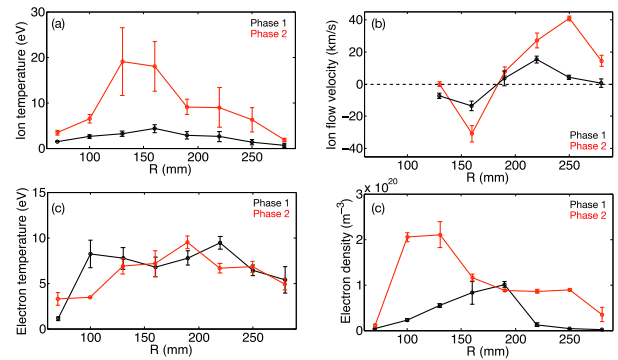


Fig. 5 Radial profiles of (a) ion temperature  $T_i$ , (b) ion flow velocity  $V_i$ , (c) electron temperature  $T_e$ , and (d) electron density  $n_e$  at  $Z = 0 \text{ mm}$  in the direction of the reconnection outflow. Black and red lines represent the profiles during phase 1 and phase 2 of reconnection, respectively. X-point is  $R \sim 190 \text{ mm}$ .

$$\mathbf{H} = \frac{5}{2} n k_B T \mathbf{V}, \quad (3)$$

$$\mathbf{P}_{\text{wave}} = \tilde{\mathbf{E}} \times \tilde{\mathbf{B}} / \mu_0 = \tilde{E}_\theta \tilde{B}_Z / \mu_0 \text{ (out)}, \quad (4)$$

where  $\mathbf{P}_{\text{mag}}$  is the Poynting flux,  $\mathbf{K}$  is the kinetic energy flux,  $\mathbf{H}$  is the thermal energy flux, and  $\mathbf{P}_{\text{wave}}$  is the wave (fluctuation) energy flux. The incoming wave energy flux is not considered because no significant fluctuation is observed in the inflow region. Note that electrostatic fluctuations  $\tilde{E}_\theta$  are measured by a double Langmuir probe at  $R = 160 \text{ mm}$  where the largest electromagnetic fluctuations were measured (not shown).

Figure 6 shows the definition of the inflow and outflow regions employed to calculate incoming and outgoing energy fluxes through the diffusion region. Under the assumption that the radial profiles of the incoming flux and axial profiles of the outgoing flux are uniform at the inlet/outlet locations of the diffusion region, the energy flows per unit time  $W$  can be calculated by the following equations:

$$W_{\text{mag}} = \int_S \mathbf{P}_{\text{mag}} \cdot d\mathbf{s}, \quad (5)$$

$$W_{\text{kin}} = \int_S \mathbf{K} \cdot d\mathbf{s}, \quad (6)$$

$$W_{\text{the}} = \int_S \mathbf{H} \cdot d\mathbf{s}, \quad (7)$$

$$W_{\text{wave}} = \int_S \mathbf{P}_{\text{wave}} \cdot d\mathbf{s}. \quad (8)$$

Integration areas  $S$  for incoming and outgoing are defined as  $S_{\text{in}} = \pi(R_1^2 - R_2^2)$  and  $S_{\text{out}} = 2\pi R_{\text{out}} \delta$ , respectively. Here, the sheet length  $L = R_1 - R_2 = 60 \text{ mm}$ , the sheet width  $\delta \sim 30 \text{ mm}$ , and  $R_{\text{out}} = 160 \text{ mm}$  is the radial location of outflow boundary as shown in Fig. 6. The assumptions at the inflow/outflow boundary of  $T_i$ ,  $V_i$ ,  $T_e$ , and  $n_e$  are generally proper for this energy inventory because their measured parameters are spatially averaged in  $30 \text{ mm}$  due to

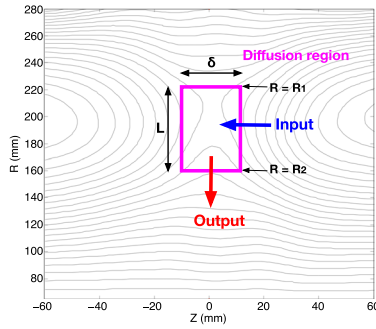


Fig. 6 Boundary of the reconnection region employed for the energy flow analysis. Gray lines represent the magnetic field lines. The incoming (blue arrow) and outgoing (red arrow) energy flow fluxes are assumed to be transferred through the diffusion region shown as the area defined by the pink line. The outlet of the diffusion region was set to be  $R_2 = 160$  and  $R_1 = 220$  mm. Radially uniform profiles for the incoming flux and axially uniform profiles for the outgoing flux are assumed at the inlet/outlet locations of the diffusion region.

Table 1 Energy investigation in phase 1 ( $t = 193 - 194 \mu\text{s}$ ).

Power [MW]	Input	Output	$\Delta W$
$W_{\text{mag}}$	3.0	0.8	-2.2
$W_{\text{the},i}$	0.08	0.05	-0.03
$W_{\text{the},e}$	0.20	0.16	-0.04
$W_{\text{kin},i}$	< 0.01	< 0.01	$\sim 0$
$W_{\text{wave}}$	N/A	0.05	0.05
$W_{\text{total}}$	3.28	1.06	-2.22

the spatial resolutions of the measurements.

Table 1 shows the energy investigation in phase 1 (fast reconnection phase). Note that the electron kinetic energy  $W_{\text{kin},e}$  is negligible because the electron mass is much smaller than the ion mass in this experiment. The plasma quantities at the inflow region are measured at  $Z = 15$  mm and  $R = 190$  mm. As shown in Table 1, the wave energy per unit time  $W_{\text{wave}}$  is approximately 0.05 MW, which is approximately 1.5% of the incoming magnetic energy per unit time  $W_{\text{mag},\text{in}}$  (3.0 MW). The dissipated magnetic energy per unit time  $\Delta W_{\text{mag}} = W_{\text{mag},\text{in}} - W_{\text{mag},\text{out}}$  is evaluated to be 2.2 MW. Therefore, 2.5% of the dissipated magnetic energy is converted into the wave energy. Ions and electrons still do not gain energy significantly. This result indicates that waves do not contribute to ion and electron heating in the downstream region. The total dissipated energy ( $\Delta W_{\text{total}} \sim 2.22$  MW) generally corresponds to the energy accumulation ( $\eta J_{\theta}^2 \sim 2.0$  MW) inside the diffusion region.

In phase 2 (the latter phase of reconnection), ion and electron gain energy eventually as shown in Table 2. In particular, the thermal energy gain of ions ( $\Delta W_{\text{the},i} = 0.5$  MW) is five times larger than that of the electrons

Table 2 Energy investigation in phase 2 ( $t = 196 - 197 \mu\text{s}$ ).

Power [MW]	Input	Output	$\Delta W$
$W_{\text{mag}}$	1.5	0.7	-0.8
$W_{\text{the},i}$	0.25	0.75	0.50
$W_{\text{the},e}$	0.20	0.30	0.10
$W_{\text{kin},i}$	< 0.01	0.1	0.1
$W_{\text{wave}}$	N/A	$\sim 0$	$\sim 0$
$W_{\text{total}}$	1.95	1.85	-0.1

( $\Delta W_{\text{the},e} = 0.1$  MW). The dissipated magnetic energy  $\Delta W_{\text{mag}}$  is approximately 0.8 MW. Therefore, 60% of the magnetic energy is converted to ion energy, and 12% of the magnetic energy is converted to electron energy. The ion kinetic energy per unit time  $W_{\text{kin},i}$  is 0.1 MW, which is five times smaller than the thermal energy gain of ions. The contribution of the kinetic energy is not dominant for the ion heating at this region.

In summary, the mechanisms of the energy conversion, with focus on the electromagnetic fluctuations during guide field magnetic reconnection ( $B_{\text{guide}}/B_{\text{rec}} \sim 2.5$ ), have been investigated experimentally in the TS-3 plasma merging device. Electromagnetic fluctuations are observed inside the current sheet and propagate to the downstream region during fast reconnection. The fluctuations might cause fast reconnection because the fast reconnection occurs when the fluctuations are observed. The fluctuations energy that propagated away from the reconnection region is 2.5% of the dissipated magnetic energy during fast reconnection (phase 1). Ions and electrons gain energy in the latter phase of magnetic reconnection (phase 2). In particular, ions significantly gain energy, which is approximately 60% of the dissipated magnetic energy. Electrons gain energy approximately 12% of the dissipated magnetic energy. However, ion kinetic energy observed during the reconnection phase is not high enough to provide ion heating. Although our estimations are spatially averaged by the assumptions and measurement resolutions in the scale of the diffusion region, it is revealed that wave energy are not comparable to the ion and electron energy gains. The fluctuations do not directly affect the energy conversion processes but enhance the reconnection rate leading to the rapid release of magnetic energy.

This work was supported in partial by Grant-in-Aid for Scientific Research (KAKENHI) 22246119, 22686085, 26287143, 25820434, and 15H05750, JSPS A3 Foresight Program ‘‘Innovative Tokamak Plasma Startup and Current Drive in Spherical Torus’’, and JSPS Core-to-Core Program 22001.

- [1] M. Yamada, R. Kulsrud and H. Ji, Rev. Mod. Phys. **82**, 603 (2010).
- [2] E.G. Zweibel and M. Yamada, Annu. Rev. Astron. Astrophys. **47**, 291 (2009).

- [3] P.A. Sweet, *Electromagnetic Phenomena in Cosmical Physics*, edited by B. Lehnert (Cambridge University Press, New York, 1958), p.123.
- [4] E.N. Parker, *J. Geophys. Res.* **62**, 509 (1957).
- [5] S. Tsuneta, H. Hara, T. Shimizu, L.W. Acton, K.T. Strong, H.S. Hudson and Y. Ogawara, *Publ. Astron. Soc. Jpn.* **44**, L63 (1992).
- [6] S. Masuda, T. Kosugi, H. Hara, S. Tsuneta and Y. Ogawara, *Nature* **371**, 495 (1994).
- [7] R. Horiuchi and T. Sato, *Phys. Plasmas* **6**, 4565 (1999).
- [8] H. Ji, S. Terry, M. Yamada, R. Kulsrud, A. Kuritsyn and Y. Ren, *Phys. Rev. Lett.* **92**, 115001 (2004).
- [9] C.C. Chaston, J.R. Johnson, M. Wiber, M. Acuna, M.L. Goldstein and H. Reme, *Phys. Rev. Lett.* **102**, 015001 (2009).
- [10] S.R. Cranmer, G.B. Field and J.L. Kohl, *Astrophys. J.* **518**, 937 (1999).
- [11] A. Kuwahata, H. Tanabe, S. Ito, M. Inomoto and Y. Ono, *Plasma Fusion Res.* **6**, 1201127 (2011).
- [12] A. Kuwahata, H. Tanabe, S. Ito, M. Inomoto and Y. Ono, *IEEEJ Trans. FM* **132**, 1 (2012).
- [13] M. Inomoto, A. Kuwahata, H. Tanabe and Y. Ono, *Phys. Plasmas* **20**, 061209 (2013).
- [14] A. Kuwahata, H. Igami, E. Kawamori, Y. Kogi, M. Inomoto and Y. Ono, *Phys. Plasmas* **21**, 102116 (2014).
- [15] G. Fiksel, D.J.D. Hartog and P.W. Fontana, *Rev. Sci. Instrum.* **69**, 2024 (1998).
- [16] H. Tanabe, A. Kuwahata, H. Oka, M. Annoura, H. Koike, N. Nishida, S. You, Y. Narushima, A. Balandin, M. Inomoto and Y. Ono, *Nucl. Fusion* **53**, 093027 (2013).
- [17] Y. Ono, M. Yamada and T. Akao, *Phys. Rev. Lett.* **76**, 3328 (1996).
- [18] J. Yoo, M. Yamada, H. Ji and C.E. Myers, *Phys. Rev. Lett.* **110**, 215007 (2013).